Higher-order vector beams produced by photonic-crystal lasers

AUTHOR(S):

Iwahashi, Seita; Kurosaka, Yoshitaka; Sakai, Kyosuke; Kitamura, Kyoko; Takayama, Naoki; Noda, Susumu

CITATION:

Iwahashi, Seita ...[et al]. Higher-order vector beams produced by photonic-crystal lasers. Optics Express 2011, 19(13): 11963-11968

ISSUE DATE:

2011

URL:

http://hdl.handle.net/2433/143574

Higher-order vector beams produced by photonic-crystal lasers

Seita Iwahashi,[1,*] Yoshitaka Kurosaka,[1] Kyosuke Sakai,[1,2] Kyoko Kitamura,[1] Naoki Takayama,[1] and Susumu Noda[1,3]

[1]*Department of Electronic Science and Engineering, Kyoto University, Kyoto-Daigaku-Katsura, Nishikyo-ku, Kyoto 615-8510, Japan*
[2]*Pioneering Research Unit for Next Generation, Kyoto University, Goryo Ohara, 1-39, Nishikyo-ku, Kyoto 615-8245, Japan*
[3]*Photonics and Electronics Science and Engineering Center, Kyoto University, Kyoto-Daigaku-Katsura, Nishikyo-ku, Kyoto 615-8510, Japan*
**iwahashi@qoe.kuee.kyoto-u.ac.jp*

Abstract: We have successfully generated vector beams with higher-order polarization states using photonic-crystal lasers. We have analyzed and designed lattice structures that provide cavity modes with different symmetries. Fabricated devices based on these lattice structures produced doughnut-shaped vector beams, with symmetries corresponding to the cavity modes. Our study enables the systematic analysis of vector beams, which we expect will lead to applications such as high-resolution microscopy, laser processing, and optical trapping.

OCIS codes: (050.5298) Photonic crystals; (140.3300) Laser beam shaping; (140.7270) Vertical emitting lasers.

References and links

1. K. Sakai and S. Noda, "Optical trapping of metal particles in doughnut-shaped beam emitted by photonic-crystal laser," Electron. Lett. **43**(2), 107–108 (2007).
2. Q. Zhan, "Trapping metallic Rayleigh particles with radial polarization," Opt. Express **12**(15), 3377–3382 (2004).
3. Y. Kozawa and S. Sato, "Focusing property of a double-ring-shaped radially polarized beam," Opt. Lett. **31**(6), 820–822 (2006).
4. K. Kitamura, K. Sakai, and S. Noda, "Sub-wavelength focal spot with long depth of focus generated by radially polarized, narrow-width annular beam," Opt. Express **18**(5), 4518–4525 (2010).
5. H. F. Wang, L. P. Shi, B. Luk'yanchuk, C. Sheppard, and C. T. Chong, "Creation of a needle of longitudinally polarized light in vacuum using binary optics," Nat. Photonics **2**(8), 501–505 (2008).
6. Y. Kozawa and S. Sato, "Sharper focal spot formed by higher-order radially polarized laser beams," J. Opt. Soc. Am. A **24**(6), 1793–1798 (2007).
7. V. G. Niziev and A. V. Nesterov, "Influence of beam polarization on laser cutting efficiency," J. Phys. D **32**(13), 1455–1461 (1999).
8. Y. Kurosaka, S. Iwahashi, Y. Liang, K. Sakai, E. Miyai, W. Kunishi, D. Ohnishi, and S. Noda, "On-chip beam-steering phtonic-crystal lasers," Nat. Photonics **4**(7), 447–450 (2010).
9. S. C. Tidwell, G. H. Kim, and W. D. Kimura, "Efficient radially polarized laser beam generation with a double interferometer," Appl. Opt. **32**(27), 5222–5229 (1993).
10. R. Oron, S. Blit, N. Davidson, A. Friesem, Z. Bomzon, and E. Hasman, "The formation of laser beams with pure azimuthal or radial polarization," Appl. Phys. Lett. **77**(21), 3322–3324 (2000).
11. Z. Bomzon, G. Biener, V. Kleiner, and E. Hasman, "Radially and azimuthally polarized beams generated by space-variant dielectric subwavelength gratings," Opt. Lett. **27**(5), 285–287 (2002).
12. G. Volpe and D. Petrov, "Generation of cylindrical vector beams with few-mode fibers excited by Laguerre-Gaussian beams," Opt. Commun. **237**(1–3), 89–95 (2004).
13. Y. Kozawa, S. Sato, T. Sato, Y. Inoue, Y. Ohtera, and S. Kawakami, "Cylindrical vector laser beam generated by the use of a photonic crystal mirror," Appl. Phys. Express **1**(2), 022008 (2008).
14. H. Kawauchi, Y. Kozawa, S. Sato, T. Sato, and S. Kawakami, "Simultaneous generation of helical beams with linear and radial polarization by use of a segmented half-wave plate," Opt. Lett. **33**(4), 399–401 (2008).
15. E. Miyai, K. Sakai, T. Okano, W. Kunishi, D. Ohnishi, and S. Noda, "Photonics: lasers producing tailored beams," Nature **441**(7096), 946 (2006).
16. M. Imada, S. Noda, A. Chutinan, T. Tokuda, M. Murata, and G. Sasaki, "Coherent two-dimensional lasing action in surface-emitting laser with triangular-lattice photonic crystal structure," Appl. Phys. Lett. **75**(3), 316–318 (1999).

#144559 - $15.00 USD Received 21 Mar 2011; revised 7 May 2011; accepted 7 May 2011; published 6 Jun 2011

17. S. Noda, M. Yokoyama, M. Imada, A. Chutinan, and M. Mochizuki, "Polarization mode control of two-dimensional photonic crystal laser by unit cell structure design," Science **293**(5532), 1123–1125 (2001).
18. D. Ohnishi, T. Okano, M. Imada, and S. Noda, "Room temperature continuous wave operation of a surface-emitting two-dimensional photonic crystal diode laser," Opt. Express **12**(8), 1562–1568 (2004).
19. K. Sakai, E. Miyai, and S. Noda, "Coupled-wave model for square-lattice two-dimensional photonic crystal with transverse-electric-like mode," Appl. Phys. Lett. **89**(2), 021101 (2006).
20. M. Yokoyama and S. Noda, "Finite-difference time-domain simulation of two-dimensional photonic crystal surface-emitting laser," Opt. Express **13**(8), 2869–2880 (2005).
21. W. Streifer, D. R. Scifres, and R. D. Burnham, "Coupling coefficients for distributed feedback single- and double-heterostructure diode lasers," IEEE J. Quantum Electron. **11**(11), 867–873 (1975).

1. Introduction

Vector beams, which possess an inhomogeneous distribution of polarization directions, have attracted much attention because they can provide novel functional properties at their focus. For example, azimuthally polarized ring-shaped vector beams enable the optical trapping of metal particles [1–3], and radially polarized beams are expected to produce sharp focal spots [4–6]. These characteristics are expected to be useful in various fields of biological science and material science [7,8]. Several methods have been proposed for the generation of such vector beams [9–15], among which we believe that photonic crystal (PC) surface-emitting lasers (Fig. 1) [16–19] are highly promising because they can directly produce vector beams from a small laser diode chip. We have already demonstrated the direct emission of radially and azimuthally polarized vector beams from a device based on a square-lattice PC, utilizing transverse magnetic (TM) and transverse electric (TE) modes, respectively [15]. The next challenge is the generation of vector beams with other polarization states, which may attract both academic and industrial interest. Here, we investigate the potential of PC lasers to produce novel types of vector beams by altering the design of the PC. It is expected that the characteristics of vector beams are essentially determined by the symmetry of the cavity mode that the PC structure provides.

In Section 2, we analyze some basic properties of PC cavities such as the symmetries of the fundamental waves and the electromagnetic fields generated by three different PC structures, and we demonstrate their potential to produce vector beams. In Section 3, we discuss the characteristics of the output beams obtained from fabricated devices based on these structures including beam patterns and polarization. Finally, concluding remarks are given in Section 4.

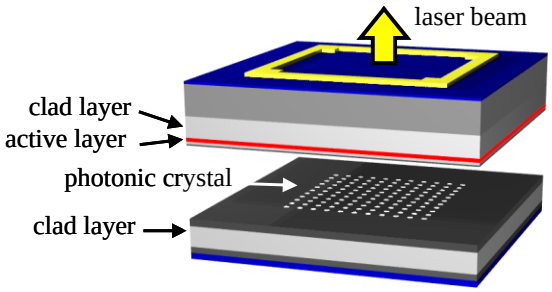

Fig. 1. Schematic structure of photonic crystal laser.

2. Photonic crystal design

We discuss three kinds of PC structures (shown in Figs. 2(a)–2(c)) that we have designed to produce vector beams: (a) the square lattice structure, which we have previously analyzed [15]; (b) the triangular lattice and (c) the square lattice with a longer lattice period. Here, we set the filling factor to be 12% for structures (a) and (b), and 3% for (c). The PC consists of a periodic distribution of air holes ($\varepsilon = 1.0$) within a GaAs host material ($\varepsilon = 12.89$).

#144559 - $15.00 USD Received 21 Mar 2011; revised 7 May 2011; accepted 7 May 2011; published 6 Jun 2011

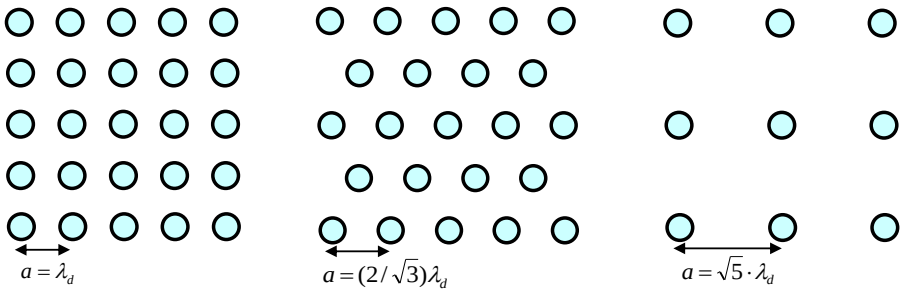

Fig. 2. Three types of photonic crystal structure considered in this paper. (a) Square lattice, where the lattice constant (a) is equal to the wavelength in the medium (λ_d). (b) Triangular lattice and (c) square lattice with larger lattice constant.

2.1. Reciprocal lattice space and fundamental waves

In order to understand the resonant mode of each lattice structure in Fig. 2, we first discuss the fundamental waves of the cavity modes in reciprocal lattice space, which are shown in Figs. 3(a)–3(c). Superscripts have been assigned to each Γ-point in order of increasing distance from the origin of reciprocal space. The yellow arrows represent the fundamental waves of the cavity modes of interest in this paper. For each of the three lattice types, the fundamental waves at identical Γ-points are equivalent; they can thus couple with each other by the reciprocal lattice vectors and produce cavity modes [19]. That is, the square lattice in Fig. 3(a) has 4 equivalent fundamental waves at the $\Gamma^{(2)}$ point, whereas the triangular lattice in Fig. 3(b) has 6 equivalent waves at the $\Gamma^{(2)}$ point and the square lattice in Fig. 3(c) has 8 equivalent waves at the $\Gamma^{(5)}$ point. In order to obtain the same lasing wavelength (λ_d) for each structure, the lattice constant (a) is designed in such a way that the magnitude of the fundamental waves ($2\pi/\lambda_d$) is identical. For example, in Fig. 3(a), the magnitude of the fundamental waves is equal to the shortest distance between the reciprocal lattice points (b); because $b = 2\pi/a$ for the square lattice structure, the lattice constant is determined as $a = \lambda_d$. In the same way, the magnitudes of the fundamental waves in Figs. 3(b) and 3(c) are expressed as

$$\frac{2\pi}{\lambda_d} = b = \frac{4\pi}{\sqrt{3}a}, \tag{1}$$

and

$$\frac{2\pi}{\lambda_d} = \sqrt{5}b = \sqrt{5}\frac{2\pi}{a}, \tag{2}$$

respectively. Therefore, the lattice constants in Figs. 2(b) and 2(c) are determined as

$$a = \frac{2}{\sqrt{3}}\lambda_d, \tag{3}$$

and

$$a = \sqrt{5}\lambda_d, \tag{4}$$

respectively. Because each set of fundamental waves possesses different symmetry, the respective optical characteristics such as the photonic band structure, electromagnetic field distribution, and beam polarization should be symmetry dependent. We calculate these characteristics in Section 2.2 using the plane wave expansion method.

#144559 - $15.00 USD Received 21 Mar 2011; revised 7 May 2011; accepted 7 May 2011; published 6 Jun 2011

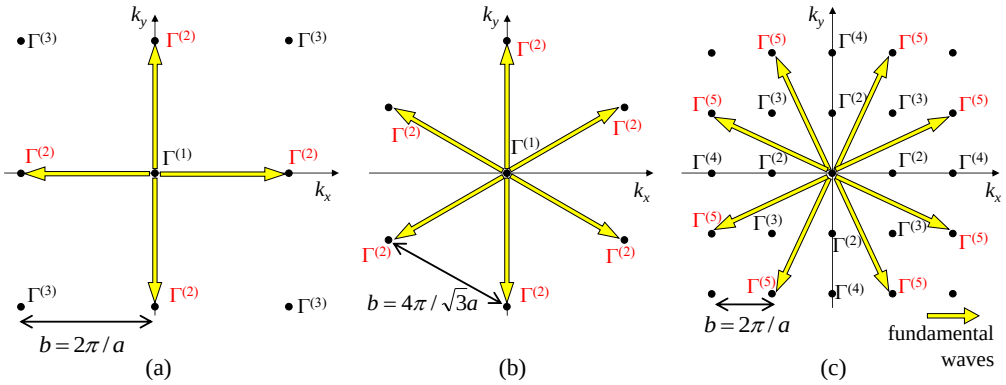

Fig. 3. Reciprocal space representations of (a) square lattice with 4 fundamental waves at lowest-order $\Gamma^{(2)}$ points, (b) triangular lattice with 6 fundamental waves at lowest-order $\Gamma^{(2)}$ points, and (c) square lattice with 8 fundamental waves at higher-order $\Gamma^{(5)}$ points.

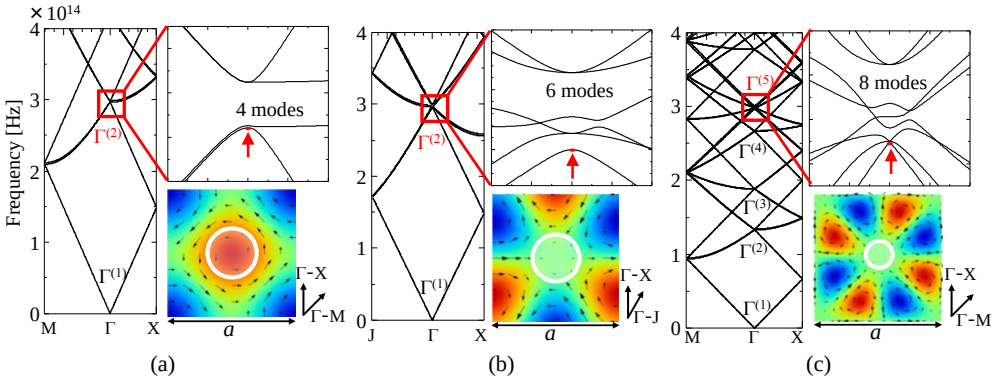

Fig. 4. Photonic band structures corresponding to the lattice structures in Figs. 2(a)–2(c). The enlarged band structure in the region enclosed by the red square is the band edge where Γ-point oscillation with the fundamental waves shown in Fig. 3 is produced. The mode numbers, denoted by superscripts, correspond to the number of fundamental waves. Corresponding electromagnetic field distributions of the unit cell in the PC plane are shown for the modes of lowest frequency, indicated by red arrows in the enlarged band diagrams. The color scale represents magnetic field and the black arrows indicate electric field. A white circle indicates the lattice hole of a PC.

2.2. Photonic band diagram and electromagnetic field calculation

Figures 4(a)–4(c) show the photonic band diagrams of the TE mode for the PC structures shown in Figs. 2(a)–2(c), respectively. The fundamental waves shown in Fig. 3 provide cavity modes at the Γ-points of interest, indicated by red squares in the band structures of Fig. 4. We can confirm from the enlarged band diagrams that in each case the number of modes at the Γ-point corresponds to the number of fundamental waves: 4 modes for (a), 6 modes for (b), and 8 modes for (c). The individual modes have particular electromagnetic field distributions in the PC plane [20] each capable of producing a vector beam. The field distributions of the lowest frequency modes indicated by the red arrows are shown in the lower right insets. These distributions reflect the symmetry of the fundamental waves. For example, in Fig. 4(a), the electromagnetic field possesses 4-fold rotational symmetry, whereas in Figs. 4(b) and 4(c), 6 and 8 magnetic field antinodes (red and blue) are distributed around the lattice hole. The output beam is emitted in the direction normal to the PC surface by the PC diffraction effect [8,18]. Therefore, the beam pattern can be determined by taking the Fourier transformation of

#144559 - $15.00 USD Received 21 Mar 2011; revised 7 May 2011; accepted 7 May 2011; published 6 Jun 2011

the electromagnetic field distribution, reflecting the symmetry of the system. If lasing oscillation arises from these cavity modes, one may expect vector beams with the corresponding symmetry of polarization to be produced. We note that the TM mode shows similar characteristics to the TE mode with respect to the number of band edges and cavity symmetry (see Appendix).

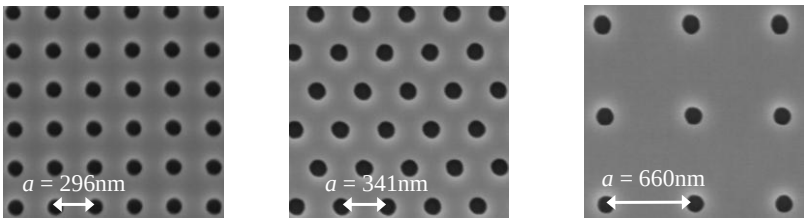

Fig. 5. Scanning electron microscope images of fabricated photonic crystals. (a) Square lattice with a = 296nm, (b) triangular lattice with a = 341nm, (c) square lattice with a = 660nm.

3. Experimental results

We have fabricated GaAs-based lasers with the PC structures designed in Section 2, using previously reported device parameters [18]. Figures 5(a)–5(c) show scanning electron microscope images of the fabricated PCs, which correspond to the structures in Figs. 2(a)–2(c). In order to obtain band-edge lasing oscillation at 980nm, the lattice constants were set as follows: (a) a = 296 nm, (b) a = 341 nm, (c) a = 660 nm. When pulsed current (1 kHz duty cycle and 500 ns pulse width) was injected, we achieved single-mode lasing oscillation with a threshold current of (a) 30 mA, (b) 30 mA, and (c) 200 mA. The higher threshold current for (c) is due to the smaller feedback strength (coupling constant) [21] at the higher-order Γ-point. The beam patterns and the polarization directions of the output beams obtained from these fabricated devices are shown in Figs. 6(a)–6(c). Vector beams of doughnut shape with small divergence angles of approximately 1° were obtained from each PC laser. The beam patterns recorded through the polarizer showed different numbers of multiple lobes: 2 lobes for (a), 4 lobes for (b), and 6 lobes for (c). This implies that the polarization direction along the circumference of the doughnut beam rotates once for (a), twice for (b), and three times for (c). The directions and symmetries of the beam polarization correspond well to the calculated electric field around a lattice hole, shown in Fig. 4 and Fig. 7. Thus, we have successfully generated higher-order vector beams with small divergence angles directly from a laser diode chip.

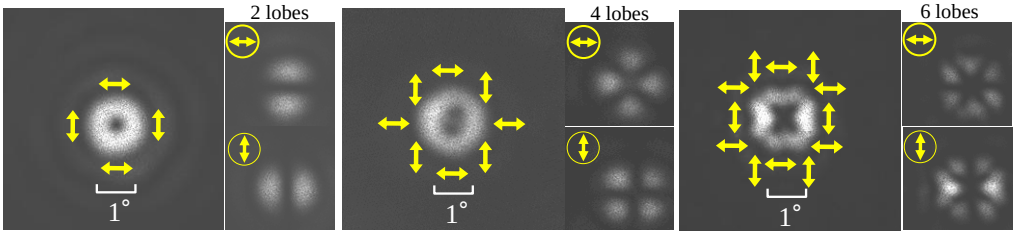

Fig. 6. Beam patterns obtained from fabricated devices with the PC structures shown in Figs. 5(a)–5(c). Yellow arrows indicate the electric field direction. For each device, the two panels on the right-hand side show the intensity pattern after passing through a polarizer. According to the multiple-lobe patterns, the polarization direction along the circumference of the doughnut beam rotates once for (a), twice for (b), and three times for (c).

#144559 - $15.00 USD Received 21 Mar 2011; revised 7 May 2011; accepted 7 May 2011; published 6 Jun 2011

4. Conclusion

We have analyzed cavity modes at the Γ-points of square and triangular lattice photonic crystals, not only for the fundamental order but also for higher-order band edges. The symmetry of the fundamental waves is important in establishing the basic laser characteristics because it determines the number of band edges and the symmetry of the electromagnetic field. The beam patterns obtained from the three devices that we have designed and fabricated were doughnut-shaped with small divergence angles of approximately 1°. The polarization direction is rotated between one and three times along the circumference of the doughnut depending on the symmetry of the photonic crystal structure. Therefore, we have succeeded in the generation of various novel vector beams, including higher-order beams. The design of such vector beams based on the cavity symmetry of photonic-crystal lasers will facilitate further variation and systematization of vector beams, which will in turn lead to versatile applications such as high-resolution microscopy, advanced laser processing and optical trapping.

Appendix: Band structure and electromagnetic field for TM mode

In Fig. 7 we show the photonic band diagrams and electromagnetic field distributions for the TM mode, in analogous fashion to those for the TE mode in Fig. 4. The electromagnetic field distributions are shown for the lowest frequency modes indicated by red arrows. The color scale represents the electric field and the black arrows indicate the magnetic field. These field distributions reflect the symmetry of the systems in a similar way to the TE mode, although the electric and magnetic fields are inverse in the two cases.

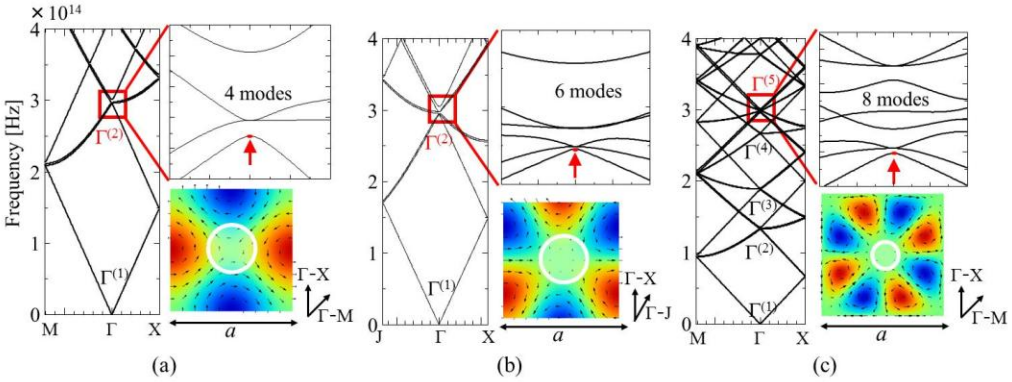

Fig. 7. Photonic band structures and electromagnetic field distributions of the TM mode for the PC structures shown in Figs. 2(a)–2(c). In the electromagnetic field distributions, the color scale represents electric field and the black arrows indicate magnetic field.

Acknowledgments

This work was partly supported by the Japan Society of Promotion and Science, the Global COE program of Kyoto University, and by Special Coordination Funds for Promoting Science and Technology (SCF) commissioned by the Ministry of Education, Culture, Sports, Science and Technology (MEXT) of Japan.

#144559 - $15.00 USD Received 21 Mar 2011; revised 7 May 2011; accepted 7 May 2011; published 6 Jun 2011